

# Multiparameter Sensitivity Analysis of Supercooled Large Droplet Icing

DENG Tian<sup>1,2\*</sup>, WANG Jiaqi<sup>1</sup>, LIU Feiyu<sup>1</sup>

1. Sino-European Institute of Aviation Engineering, Civil Aviation University of China, Tianjin 300300, P. R. China;

2. Key Laboratory of Icing and De-icing, China Aerodynamics Research and Development Center, Mianyang 621000, P.R. China

(Received 26 March 2023; revised 25 June 2023; accepted 5 August 2023)

**Abstract:** The phenomenon of supercooled large droplets (SLD) icing poses a severe threat to the safe operation of aircraft. The Sobol sequence sampling method, radial basis function (RBF) method, and Sobol's sensitivity index analysis method are used to conduct a multiparameter sensitivity analysis of SLD icing. The influence of four parameters, including icing surface roughness, presence or absence of evaporation, droplet size distribution, and the number of shots, on the shape and amount of icing formation is analyzed. The first-order sensitivity index is used to determine the degree of influence of each parameter on the ice shape parameters, and the total sensitivity index is used to compare the influence of parameter interactions on the ice shape or amount of icing formation. It is found that there is a consistent sensitivity law of the ice shape characteristic parameters of the leading edge of the airfoil to the four parameters, all of which are most affected by the roughness of the icing surface, with a total sensitivity index of more than 0.476. The number of shots has the least effect, with a total sensitivity index of about 0.2, while the remaining parameters are affected by evaporation, droplet size distribution, in the descending order.

**Key words:** airfoil icing; supercooled large droplets; sensitivity analysis; ice shape characteristic parameters

**CLC number:** V211.41      **Document code:** A      **Article ID:** 1005-1120(2023)04-0420-14

## 0 Introduction

When aircraft fly through a cloud layer of supercooled droplets, the droplets attach and freeze on the surface of the aircraft, presenting a significant hazard to safe operation<sup>[1-2]</sup>. The size, position, and shape of icing on the aerodynamic surface of the aircraft without thermal protection are primarily influenced by airspeed, temperature, droplet size, liquid water content, angle of attack, and the duration of flight of the aircraft under icing conditions<sup>[3]</sup>. Currently, the median volume diameter (MVD) of water droplets commonly used in aircraft design to determine the anti-icing area is  $20\ \mu\text{m}$ <sup>[4]</sup>. Under normal icing conditions, almost all ice accumulation can be removed when the de-icing system is activated. However, this is not the case under supercooled

large droplet (SLD) conditions. SLD can impact and overflow downstream of the de-icing system, resulting in spreading ice and leading to SLD icing and large droplet icing, which have caused numerous aviation accidents with serious consequences<sup>[5]</sup>.

Miller et al.<sup>[6]</sup> investigated the impact of meteorological parameters such as liquid water content (LWC), MVD, static temperature, on ice shape in the icing research tunnel (IRT) icing wind tunnel at NASA Glenn Research Center. The study revealed that changes in meteorological parameters can significantly affect the position of ice-horn angles and mass of icing. Campbell et al.<sup>[7]</sup> utilized the experimental data of Ref.[6] to examine the sensitivity of airfoil aerodynamic degradation to meteorological parameters. They evaluated the influence of these parameters on icing geometry and defined normal-

\*Corresponding author, E-mail address: t-deng@cauc.edu.cn.

**How to cite this article:** DENG Tian, WANG Jiaqi, LIU Feiyu. Multiparameter sensitivity analysis of supercooled large droplet icing[J]. Transactions of Nanjing University of Aeronautics and Astronautics, 2023, 40(4):420-433.

<http://dx.doi.org/10.16356/j.1005-1120.2023.04.004>

ized ice-horn height, ice-horn angle angle, ice-horn angle position, ice limit, and icing mass. Wright<sup>[8-9]</sup> employed different Navier-Stokes-Fourier icing codes to calculate ice shape and aerodynamic degradation. They compared the simulation results with test results of various airfoils under different meteorological conditions to verify the accuracy of the calculations. Son et al.<sup>[10-11]</sup> explored the effects of meteorological parameters and flight conditions (LWC, MVD, free flow velocity, and temperature) on icing. Homola et al.<sup>[12]</sup> conducted numerical studies on the growth and flow field characteristics of NACA 64618 airfoil icing to investigate the effects of atmospheric temperature and droplet size changes on ice growth speed and shape. The results showed that different temperature and thermal equilibrium conditions can lead to icing of different masses and shapes. Shin et al.<sup>[13]</sup> used a combination of LEWICE icing code correction and interactive boundary layer program to calculate a wide range of values of airspeed, temperature, droplet size, liquid water content, airfoil, angle of attack, and other parameters. They developed an improved equivalent roughness correlation based on experimental data.

Zhu et al.<sup>[14]</sup> investigated the effects of droplet diameter and multi-size distribution on the impingement characteristics and ice shape of droplets. Their findings indicated that the multi-size distribution of droplets had a significant impact on the numerical simulation results of icing. Cao et al.<sup>[15]</sup> established a supercooled large droplet motion model, taking into account the effects of droplet breakup, splashing, and rebound, and conducted numerical simulations of icing. They studied the influence of boundary conditions and droplet diameter on the shape of icing. Zhou et al.<sup>[16]</sup> provided a systematic exposition of the basic concept of SLD icing on aircraft. They analyzed the primary influencing factors of different physical processes such as dynamics and thermodynamics during SLD icing, as well as the mutual influence and coupled relationship between different physical processes. They also summarized the typi-

cal differences between SLD icing and conventional droplet icing. Li et al.<sup>[17]</sup> developed a three-dimensional numerical icing simulation software named AERO-ICE. The software simulates the icing situation using four modules: Automatic mesh generation, RANS calculation of airflow field, calculation of Euler method of droplet field, and thermodynamic analysis of icing.

There are typically three methods used for the design and certification of aircraft regarding the issue of aircraft icing: Computational fluid dynamics (CFD), icing wind tunnel experiments, and flight tests. Real flight tests are limited by test site, season, and high experimental costs, while icing wind tunnel experiments are limited by complicated scaling laws, spray equipment accuracy, and excessively high LWC, making it difficult to simulate all meteorological icing conditions prescribed by the icing certification envelope of Appendices C&O. Therefore, with the advancement and development of computer software and hardware and icing simulation programs, computational fluid dynamics is playing an increasingly important role in icing experiments. Ansys FENSAP-ICE is a comprehensive engineering simulation software developed by Ansys, Inc. specifically designed for aircraft icing analysis and certification. This advanced software suite provides a robust, multi-disciplinary approach to assess the performance of aerospace systems in icing conditions, ensuring the design complies with stringent safety regulations and certification requirements. The ice shape results of this paper are all generated from the output of Ansys FENSAP-ICE.

In addition to meteorological icing parameters and flight conditions, some physical and modeling parameters in CFD icing simulations also play a crucial role in simulating aircraft surface icing. These physical and modeling parameters have also been addressed in icing simulation programs such as FENSAP-ICE and can be customized. These parameters include ice density, presence or absence of evaporation, droplet size distribution, and the number of

computational simulation shots. In earlier numerical icing simulations, setting the ice density to a constant value was a common method for saving computational resources and simplifying calculations, which still appears in the tutorials of the latest icing simulation software. However, ice density is determined by droplet impact velocity, MVD, and surface temperature, and constant ice density cannot meet the accuracy requirements of icing prediction. The latest icing simulation studies introduce empirical formulas to calculate ice density. In this case, it is generally believed that ice density is not in the same dimension as the other variables, and comparing them together lacks meaning.

Therefore, this paper studies the sensitivity of SLD icing to four key physical and modeling parameters. Its purpose is to compare the degree of influence of key physical and modeling parameters on SLD icing and provide valuable reference for future research in this field.

## 1 Sensitivity Analysis Methods

Global sensitivity analysis (GSA) is a methodology used to evaluate the sensitivity of a model's output to changes in its input parameters<sup>[18-20]</sup>. It involves varying the inputs over a range of values and observing the resulting changes in the model output. GSA can help identify which input parameters are the most important in determining the output of a model, and can also provide insights into the relationships between input and output variables. Some of the main methods used in GSA including: Morris method<sup>[21]</sup>, Sobol's method<sup>[22]</sup>, Fourier amplitude sensitivity test (FAST)<sup>[23]</sup>, extended Fourier amplitude sensitivity test (eFAST)<sup>[24]</sup>, Monte Carlo methods<sup>[25]</sup>.

The GSA method based on sampling/proxy (Metamodel) is a class of methods used for sensitivity analysis when the model itself is computationally expensive or time-consuming<sup>[26-27]</sup>. This method involves constructing a surrogate model or metamodel that approximates the behavior of the original model

using a smaller set of input-output data points. The surrogate model is then used to perform the sensitivity analysis, rather than the original model. The GSA method based on sampling can significantly improve the performance of GSA by using low-discrepancy sequences (such as Sobol sequences). The GSA method based on proxy constructs a metamodel to evaluate sensitivity indices using Sobol's method. Commonly used metamodels for constructing models include Kriging (Gaussian process regression)<sup>[28]</sup>, radial basis functions (RBF)<sup>[29]</sup>, artificial neural networks (ANN)<sup>[30]</sup>, support vector machines (SVM)<sup>[31]</sup>, etc.

In this paper, Sobol sequence sampling method is used to generate uniformly distributed sampling points within the given design space, and radial basis function (RBF) is used to construct the metamodel. Sobol's method is then used to evaluate the sensitivity indices (SSIs) of critical physics and modeling parameters in ice simulation. Similar methods for computing sensitivity indices have been validated in many literature sources<sup>[32-35]</sup>.

### 1.1 Sampling method based on Sobol sequence

Sensitivity analysis typically involves designing sampling points, constructing metamodels, and evaluating sensitivity indicators. Sampling is the process of exploring the system space, and the distribution of design points in a given system space is crucial. Generating random numbers that are evenly distributed in the system space efficiently and accurately is a critical aspect of algorithm programs. The choice of sampling strategy is an essential step in sensitivity analysis because the more uniform the distribution of random numbers, the more reliable the sample distribution is for all algorithmic programs that need to be sampled. Compared with other sampling methods such as pseudo-random numbers, Latin hypercube sampling (LHS), and stratified sampling, low discrepancy sequence generation samples have relatively higher convergence efficiency and a more uniform distribution of random numbers. This is intuitively illustrated in Fig.1.

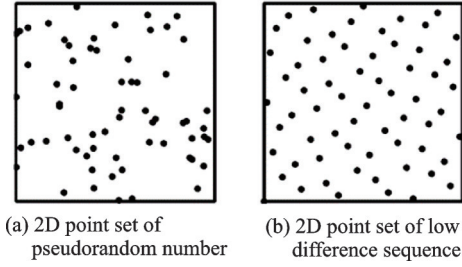


Fig.1 Comparison of uniformity of random number distribution in samples

There are several common low-variance sequences, including Van der Corput, Sobol, Hammersley, Halton, and Rank-1 lattice<sup>[36]</sup>. The Sobol sequence is a type of quasi-random sampling method, and all its dimensions are based on Radical Inversion with base 2. Since it is based on base 2, every number is extracted from binary, and matrix operations can be performed using bit operations such as right shift and XOR. This makes it very efficient and easy to generate samples with high-quality distribution, as shown in Fig.2. After dividing the sample space in various ways, the number of sample points falling in each subspace is essentially the same.

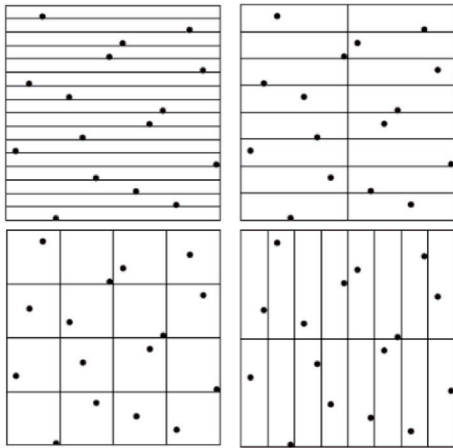


Fig.2 Sample distribution generated based on Sobol sequence

The Sobol sequence-based sampling method can evenly distribute design points across domains. Moreover, sampling methods based on Sobol sequences converge to the true mean faster than other methods<sup>[36]</sup>. Given these advantages, this paper employs Sobol sequences to generate sampling points for each icing parameter.

## 1.2 RBF method construct metamodells

The process of building a metamodel involves restoring and approximating a complete system based on the finite samples generated by the system. The RBF method was initially developed to fit irregular contours in geographic information data<sup>[37]</sup> and has a good fitting effect on deterministic and random response functions. RBF neural network approximation is a type of neural network that uses a radial element hidden layer and a linear unit output layer. It has a strong ability to approximate complex nonlinear functions, fast learning speed, and has been widely used in various industries<sup>[38]</sup>.

RBF can be expressed as

$$Y = F(\mathbf{x}) = \sum_{n=1}^N \omega_n \varphi(\|\mathbf{x} - \mathbf{x}_n\|) \quad (1)$$

where  $\varphi$ ,  $\mathbf{x}$  and  $\mathbf{x}_n$  represent the basis function vector, design variable and design variable vector of the  $n$ th sample point, respectively;  $\|\mathbf{x} - \mathbf{x}_n\|$  is the Euclidean norm of the  $n$ th basis function;  $\omega_n$  the unknown coefficient of the  $n$ th basis function. The coefficient vector  $\mathbf{w}$  can be expressed as follows

$$\mathbf{w} = \mathbf{A}^{-1} \mathbf{F} \quad (2)$$

where

$$\mathbf{w} = \begin{bmatrix} \omega_1 \\ \omega_2 \\ \vdots \\ \omega_N \end{bmatrix}, \mathbf{A} = \begin{bmatrix} \varphi_{11} & \varphi_{12} & \cdots & \varphi_{1,N} \\ \varphi_{21} & \varphi_{22} & \cdots & \varphi_{2,N} \\ \vdots & \vdots & \ddots & \vdots \\ \varphi_{N1} & \varphi_{N2} & \cdots & \varphi_{NN} \end{bmatrix}, \mathbf{F} = \begin{bmatrix} f_1 \\ f_2 \\ \vdots \\ f_N \end{bmatrix} \quad (3)$$

## 1.3 Sensitivity indices

Based on Sobol's method, the computational model is decomposed for global sensitivity analysis, which can be decomposed into the following form

$$F(\mathbf{x}) = F_0 + \sum_{N=1}^n F_N(x_N) +$$

$$\sum_{1 \leq N < M \leq n} F_{NM}(x_N, x_M) + \cdots + F_{12 \dots n}(\mathbf{x}) \quad (4)$$

where  $F_0$  is a constant;  $F_N$  a function of  $x_N$ ; and  $F_{NM}$  a function of  $x_N$  and  $x_M$ . And there are

$$\int_0^1 F_{N_1 N_2 \dots N_s}(x_{N_1}, x_{N_2}, \dots, x_{N_s}) dx_k = 0 \quad (5)$$

$$k = N_1, N_2, \dots, N_s$$

When the items satisfy the following relationships

$$F_0 = \int F(x) dx \quad (6)$$

$$F_N(x_N) = \int F(x) \prod_{K \neq N} dx_K - F_0 \quad (7)$$

$$F_{NM}(x_N, x_M) = \int F(x) \prod_{K \neq M, N} dx_K - F_0 - F_N(x_N) - F_M(x_M) \quad (8)$$

The decomposition of  $F$  is called ANOVA, where the variance of  $F(x)$  is expressed as

$$D = \int F(x)^2 dx - F_0^2 \quad (9)$$

Integrating the sum of squares on both sides of Eq.(9) yields

$$D = \sum_{i=1}^k D_i + \sum_{i < j} D_{ij} + \dots + D_{1,2,\dots,k} \quad (10)$$

where  $D_{i \dots i_i}$  is the variance of the parameter sub-model  $F_{i \dots i_i}(x_{i_1}, \dots, x_{i_i})$ , expressed as

$$D_{i \dots i_i} = \int F_{i \dots i_i}^2(x_{i_1}, \dots, x_{i_i}) dx_{i_1}, \dots, x_{i_i} \quad (11)$$

The corresponding parameter sub-models SSIs are defined as

$$S_{i \dots i_i} = \frac{D_{i \dots i_i}}{D} \quad (12)$$

Thus, the first-order sensitivity index (individual parameter influence) of any variable  $x_i$  can be defined as

$$S_i = \frac{D_i}{D} \quad (13)$$

The second-order sensitivity index (the interaction of two different parameters) can be defined as

$$S_{ij} = \frac{D_{ij}}{D} \quad (14)$$

By analogy, the total sensitivity index is defined as

$$S_{Ti} = S_i + S_{ij, i \neq j} + \dots + S_{1 \dots i \dots s} \quad (15)$$

Among them, the first-order sensitivity index is used to measure the influence of a single parameter on the output variance. The second-order sensitivity index is used to measure the interaction effect of two different parameters on the output variance. The total sensitivity index is the sum of the sensitivity indices of each order. The larger the total sensitivity index, the greater the influence of the parameter, and vice versa.

## 2 Impact of Key Physics and Modeling Parameters on Icing

In this section, all the numerical simulations of icing were conducted under the icing conditions of static temperature  $-10^\circ\text{C}$ , static pressure 101 325 Pa, incoming flow velocity of 102.88 m/s, LWC of  $1.0 \text{ g/m}^3$ , MVD of  $100 \mu\text{m}$ , and a 0.914 4 m NACA0012 airfoil with an icing time of 210 s. To compute ice shapes that are relatively realistic and accurate, a quasi-steady multi-shot approach was used. This approach divided the total time of ice accretion into smaller steady-state intervals or "shots", during which air, droplets and ice were computed on a fixed grid. At the end of each shot, a new mesh was generated to account for the additional icing deposition obtained during that shot, and this new mesh was used as the fixed grid for the next shot.

### 2.1 Effect of surface roughness

Surface roughness most commonly refers to the variations in the height of the surface relative to a reference plane. Iced surfaces develop roughness during an ice accretion process. Fig.3 briefly introduces the concept of icing surface roughness.

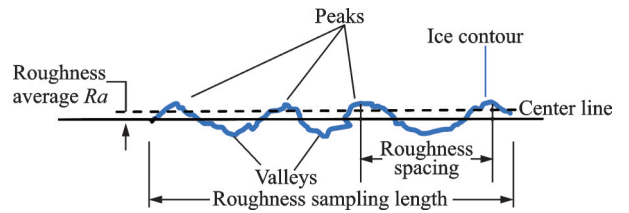


Fig.3 Sketch of iced surface roughness

The roughness that forms during the initial stages of an icing encounter is considered to be highly significant to both the overall ice accretion process and the resulting degradation in aircraft performance. This expectation is based on two facts: Firstly, the roughness enhances local convection, which leads to more rapid icing formation rates, secondly, the roughness generates local flow perturbations, which increase skin friction and may cause the boundary-layer flow to transition to turbulence prematurely. Due to its importance to the overall aircraft ice accretion process, the physical characteris-

tics of roughness and its evolution during the ice accretion process have been the subject of many investigations, including both measurement and modeling efforts.

The shear stress and heat transfer coefficient on the airfoil surface exhibit abrupt changes with variations in surface roughness. Among these, the heat transfer coefficient is particularly important for convective heat transfer and evaporative cooling. Therefore, the effect of surface roughness on the shape of icing can be directly observed, as shown in Fig.4 (Note: The range of roughness values used in this study is based on the research of Ruff et al.<sup>[39]</sup> and Shin et al.<sup>[40]</sup>).

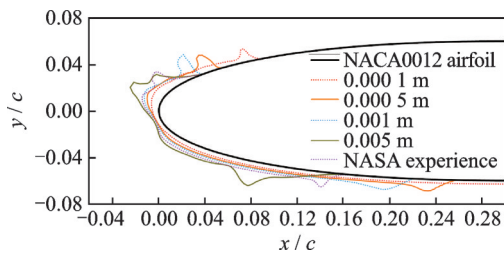


Fig.4 Ice shape comparison under different roughnesses

Fig.5 presents a comparison of the surface heat transfer coefficients of airfoils with different roughness values. It can be observed that an increase in surface roughness leads to an increase in the heat transfer coefficient of the airfoil surface, which in turn leads to an increase in the surface heat flux and severity of airfoil surface icing. When combined with Fig.4, it can be seen that an increase in surface roughness results in the gradual formation of distinct ice-horn ice at the leading edge. These two factors

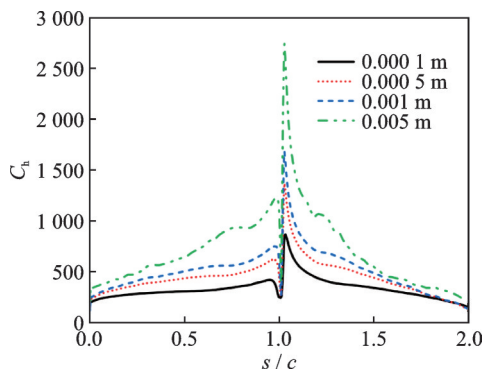


Fig.5 Comparison of heat transfer coefficient of airfoil surface with different roughnesses

are the primary reasons why the rate of ice growth is observed to increase after a thin layer of ice forms on the surface of the aircraft.

## 2.2 Effect of single-shot and multi-shots methods

In numerical icing simulation using the single-shot method, the entire icing calculation is treated as a steady-state process, where the ice shape is calculated based on the initial airflow field solution and the initial water droplet field solution. This method does not consider any mesh deformation and reconstruction caused by icing during the entire icing time. In contrast, the multi-shots method treats the entire icing calculation as a quasi-steady-state process and divides the icing time into many small segments. After each icing time, the mesh is deformed and reconstructed to adapt to the geometric changes caused by ice growth. The airflow field solution and water droplet field solution are then updated and entered into the cycle calculation. Although the complete unsteady icing method is the most accurate, it is only suitable for frosted ice and has limited application in engineering due to its dependence on a large number of computing resources. In summary, the quasi-steady-state multi-shots method is a relatively accurate numerical simulation method for icing that consumes acceptable computing resources and has been widely used. Fig.6 illustrates the difference in ice shape calculated by the single-shot and multi-shots length methods. As the multi-shots method updates the mesh, airflow field solution, and water droplet field solution after each icing time step, it can predict the ice shape more accurately than the single-shot method.

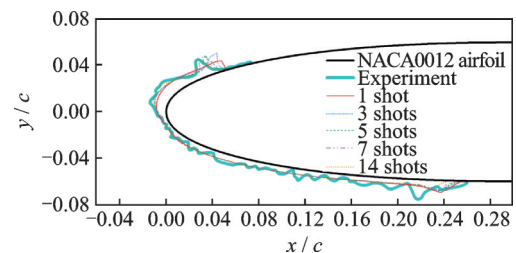


Fig.6 Comparison of ice shapes under different numbers of shots

### 2.3 Effect of droplet size distribution

In the case of multi-size distribution of droplets, the motion and impingement characteristics of each size in the water droplet field are first solved. Then, the water droplet collection rate  $\beta_i$  of each size is weighted and summed to determine the total water droplet collection rate in the water droplet field. Ref. [41] indicates that droplets of different sizes in the multi-distribution will have varying impacts, and the droplet collection rate at the impact limit caused by the splash rebound behavior of the SLD impingement wall will not be as concentrated as the single-size water droplet field. The droplet collision limit will also be extended. Under frosted icing conditions, the total temperature is low, and the droplets hitting the wall freeze immediately, so the freezing impact limit is directly determined by the water droplet impact limit. Under clear ice/glazed icing conditions, the ice limit is determined by the water film reflux phenomenon that exceeds the water droplet impact limit, but it is still positively affected by the water droplet impact limit. This is also confirmed in Fig.7, where the droplet multi-distribution extends the ice limit relative to the droplet single distribution, particularly evident for the positive angle of attack of the upper wing surface.

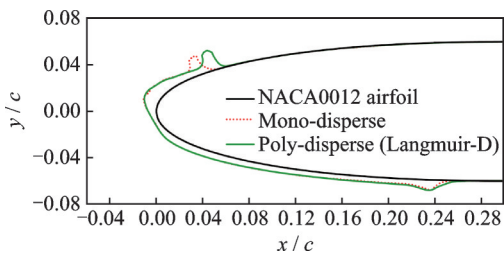


Fig.7 Comparison of ice shapes under different droplet size distributions

### 2.4 Effect of evaporation

Evaporation is an important factor influencing the amount and shape of ice accumulation, and the heat transfer associated with it is second only to convective heat transfer. Chilton et al.<sup>[42]</sup> defined the evaporation mass loss as a function of the diffusion mass transfer coefficient, and only a small fraction of the liquid water film striking the surface will evaporate

into the air. The loss of liquid water quantity due to evaporation can be expressed as

$$\dot{m}_{\text{evap}} = h_{\text{dif}}(\rho_{\text{vs}} - \rho_{\text{ve}})A \quad (16)$$

where  $h_{\text{dif}}$  is the mass transfer coefficient, expressed as

$$h_{\text{dif}} = \frac{h_c}{\rho_a C_{p,a} Le^{2/3}} \quad (17)$$

where  $\rho_{\text{vs}}$  is the saturated water vapor density at the impact surface temperature;  $\rho_{\text{ve}}$  the water vapor density at the boundary layer edge temperature;  $A$  the impact surface area, and  $Le$  is the Lewis number, which is defined as

$$Le = \frac{k_a}{\rho_a C_{p,a} D_{va}} \quad (18)$$

where  $k_a$  is the thermal conductivity of air;  $D_{va}$  the diffusion coefficient of water vapor in air; and  $C_{p,a}$  the isobaric heat capacity of air.

Fig.8 shows the difference in ice shape obtained with and without the loss of evaporated mass considered. It can be seen that the presence of evaporative mass loss significantly reduces the thickness of the leading-edge ice under the given icing conditions.

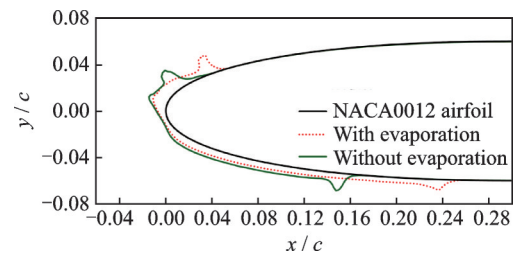


Fig.8 Effects of evaporation on ice shape

## 3 Parameter Sensitivity Analysis Based on Sobol's Method

### 3.1 Sensitivity analysis of a single parameter

In this section, the sensitivity of ice shape to these parameters is analyzed one by one to analyze which parameter has a deeper influence on ice shape, and to compare the interaction between the parameters on icing. The range of key parameters considered in the parameter sensitivity analysis in this section is shown in Table 1, with sample points generated using Sobol sequences, followed by a

model of the system using RBF metamodeling methods. The ice shape characteristic parameters of the leading edge of the airfoil are an important tool to describe the icing of supercooled droplets on the airfoil.

**Table 1** Range of key parameters

Parameter	Minimum	Maximum
Roughness/m	0.000 1	0.005
Number of shots	1	14

Ruff et al.<sup>[43]</sup> is the first to provide a geometric description of ice accretion, which mainly includes ice thickness at the stagnation point, maximum ice thickness, maximum ice width, impact limit width, ice ice-horn length, and ice ice-horn inclination angle as ice shape parameters. However, the ice shape parameters they defined have not been widely applied.

In 2012, the Society of Automotive Engineers (SAE) in the United States established some standards for icing wind tunnel tests<sup>[44]</sup> and explicitly defined ice shape parameters for quantitatively describing the two-dimensional airfoil icing geometric characteristics. These parameters include the upper and lower ice limits, upper ice-horn height, lower ice-horn height, upper ice-horn angle, and lower ice-horn angle, etc. As shown in Fig.9, the upper and the lower ice limits are the farthest positions of ice accretion on the upper and the lower surfaces of the airfoil from the stagnation point, respectively, with the upper surface being positive and the lower surface being negative. The upper (lower) ice-horn is the ice ice-horn with the maximum ice height along the normal direction on the upper (lower) surface of the airfoil. For cases with multiple ice ice-horns due to non-zero angle of attack, the upper and the lower ice-horns are defined as the ones closest to the stagnation point and with the largest ice heights on the upper and the lower surfaces, respectively. For frost with only one ice ice-horn, the upper and the lower ice-horns are still designated based on the position of the stagnation point. Furthermore, the upper (lower) ice-horn angle is defined as the angle between the line connecting the vertex of the upper

(lower) ice-horn and the leading edge of the airfoil, while the upper (lower) ice-horn height is the height from the vertex of the upper (lower) ice-horn along the normal direction to the airfoil surface.

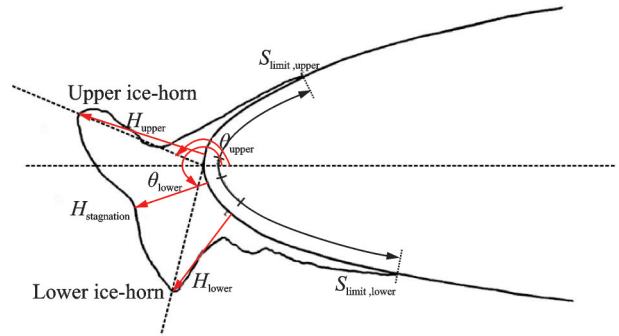


Fig.9 Airfoil icing geometric characteristics

The ice shape characteristic parameters of the leading edge of the airfoil evaluated in this paper include: Upper ice-horn height  $H_{upper}$ , lower ice-horn height  $H_{lower}$ , upper ice-horn angle  $\theta_{upper}$ , and lower ice-horn angle  $\theta_{lower}$ , upper ice limits  $S_{upper}$ , upper lower ice limits  $S_{lower}$ .

First, the sensitivity of the ice shape characteristic parameters of the leading edge of the airfoil to roughness is investigated, and the first-order sensitivity index and total sensitivity index of roughness are listed in Fig.10. It can be seen that under the condition of only considering roughness, the height of the upper and lower ice-horn angles has relatively strong sensitivity to roughness, and the sensitivity of the upper and the lower ice-horn angles and the upper and the lower ice limits to roughness is relatively insignificant. Taking into account the interaction of all parameters, the degree of roughness influence is ice-horn height (about 0.5) > ice-horn angle (about 0.4) > ice limit (about 0.3).

Second, the sensitivity to the number of shots is evaluated, and the first-order sensitivity index and the total sensitivity index of the shot number are listed in Fig.11. It can be seen that when only considering the number of shots, except for the relatively strong sensitivity of the upper and lower ice limits to the number of shots, the sensitivity of the ice shape characteristic parameters of the leading edge to the number of shots is relatively insignificant.

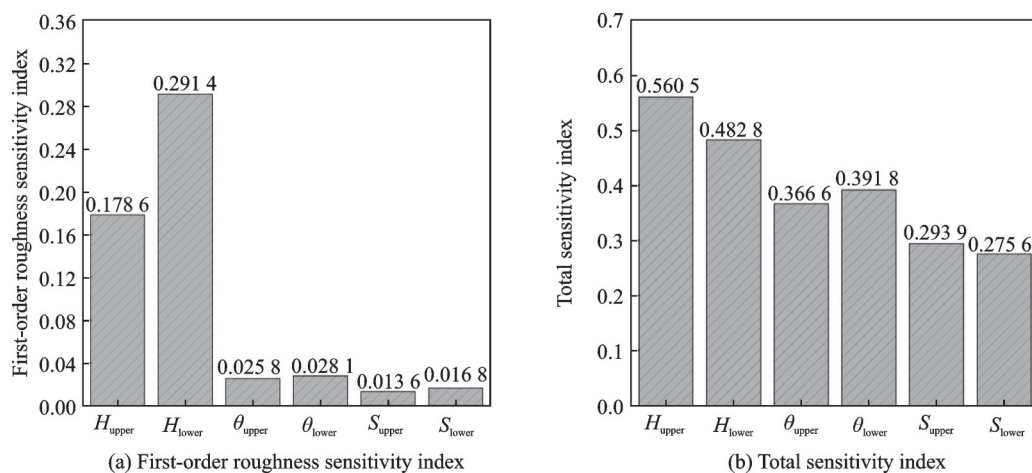


Fig.10 Comparison of sensitivity indices of leading-edge ice shape parameters to roughness

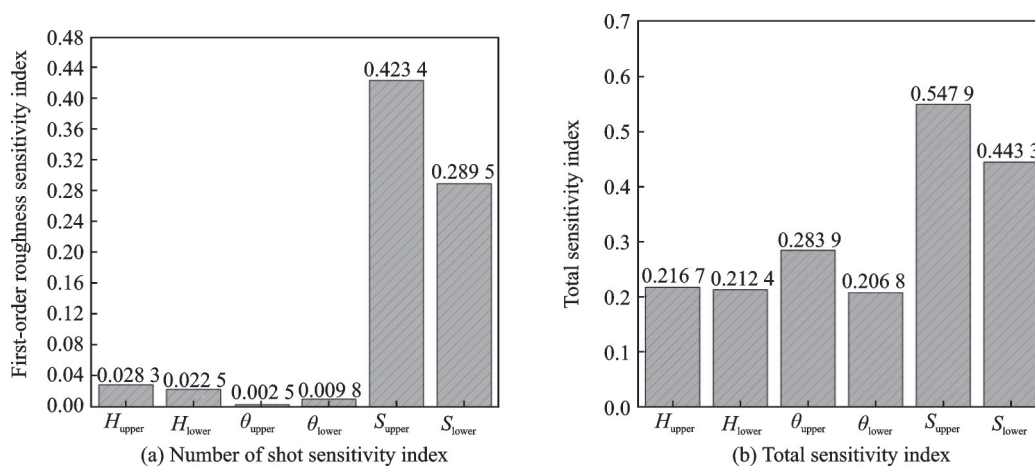


Fig.11 Comparison of sensitivity indices of leading-edge ice shape parameters to the number of shots

Taking into account the interaction of all parameters, the degree of influence of the number of shots is ice limit (about 0.5) > ice-horn angle (about 0.25) > ice-horn height (about 0.2).

The sensitivity to the droplet size distribution is then evaluated, and the first-order sensitivity index and total sensitivity index of the droplet size distribution are listed in Fig.12. It can be seen that the height of the upper and the lower ice-horn angles and the angle of the upper and the lower ice-horn angles have relatively strong sensitivity to the size distribution of water droplets when only considering the droplet size distribution, and the sensitivity of ice limits to the size distribution is relatively insignificant. Considering the mutual influence of all parameters, all the considered airfoil leading edge ice shape characteristic parameters have obvious sensitivity to the droplet size distribution, that is, the

change of the droplet size distribution has a significant impact on it, among which the degree of influence ice-horn angle (about 0.5, 0.6) > ice-horn height (about 0.35) > ice limit (about 0.3).

Finally, the sensitivity of the ice shape characteristic parameters of the leading edge of the airfoil to evaporation is evaluated, and the first-order sensitivity index and total sensitivity index of evaporation are listed in Fig.13. It can be seen from the results that in the case of only considering evaporation, except for the relatively insignificant sensitivity of the lower ice-horn angle to evaporation, the ice shape characteristic parameters have relatively strong sensitivity to evaporation. Taking into account the interaction of all parameters, the degree of evaporation influence is ice-horn angle (about 0.6) > ice-horn height (about 0.4, 0.5) > ice limit (about 0.3, 0.4).

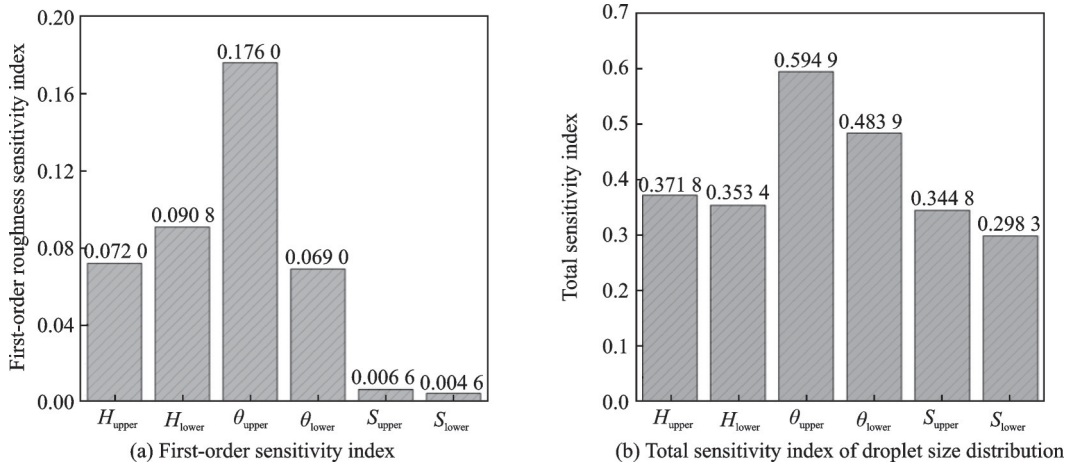


Fig.12 Comparison of sensitivity indices of leading-edge ice shape parameters to droplet size distribution patterns

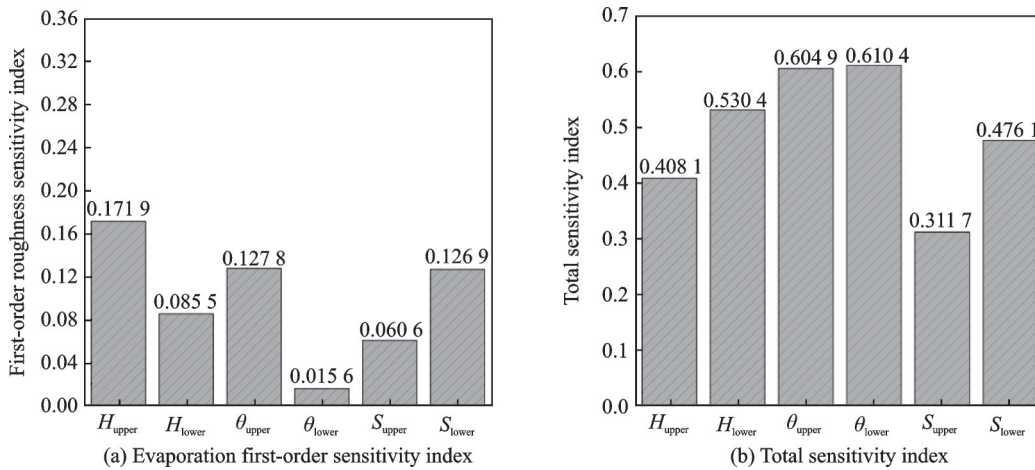


Fig.13 Comparison of sensitivity indices of leading-edge ice shape parameters to evaporation

### 3.2 Sensitivity analysis results

The total sensitivity index is an important indicator to measure the degree to which a parameter affects icing. The six main ice-horn angle characteristic parameters of the leading edge of the airfoil are compared: Upper ice-horn height  $H_{upper}$ , lower ice-horn height  $H_{lower}$ , upper ice-horn angle  $\theta_{upper}$ , and lower ice-horn angle  $\theta_{lower}$ , upper ice limits  $S_{upper}$ , upper lower ice limits  $S_{lower}$ . Their total sensitivity index is obtained for four key physical and modeling parameters: Icing surface roughness, the number of shots, droplet size distribution, and evaporation. The results are listed in order from smallest to largest, as shown in Fig.14.

The total sensitivity index of each parameter for the leading-edge ice shape parameters of the six airfoils exhibits a consistent pattern. In fact, the magnitude of the total sensitivity index represents

the relative importance of each parameter on the output response.

Therefore, we can draw the conclusion that. The degree of influence is as follows: Roughness > evaporation > droplet size distribution > the number of shots. It is observed that among the four key physical and modeling parameters studied, roughness has the greatest influence on the shape of icing, while the number of shots has the least influence.

## 4 Discussion and Conclusions

In addition to meteorological conditions, flight conditions, and dimensional conditions, there are several key physical and modeling parameters that play an important role in numerical simulations of icing. These parameters include presence or absence of evaporation, droplet size distribution, and the number of computational simulation shots. This pa-

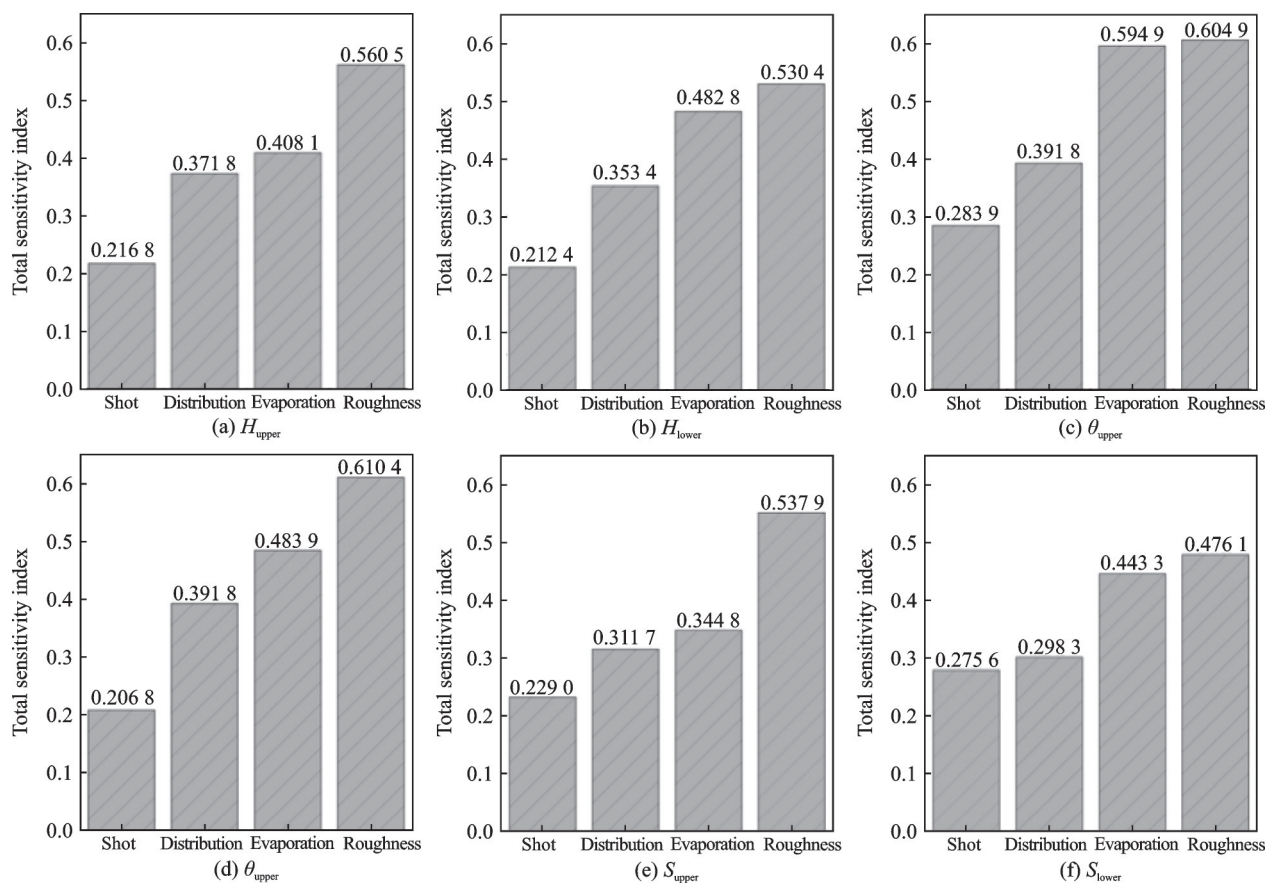


Fig.14 Comparison of the total sensitivity index of ice shape characteristic parameters of airfoil leading edge to each parameter

per first qualitatively analyzes the impact of these four parameters on SLD icing and finds that:

(1) Increased surface roughness leads to an increase in the heat transfer coefficient of the airfoil surface, that is, an increase in surface heat flux, which in turn leads to a more severe degree of airfoil surface icing.

(2) Multi-shot can more accurately predict the shape of ice accumulation compared to single-shot, and the more the number of shots, the more accurate the calculation.

(3) Under a poly-disperse distribution pattern, water droplets of different sizes will cause different impact modes, resulting in a more significant decrease in the water droplet collection rate at the impact limit caused by the splash behavior of SLD, compared to a mono-disperse water droplet field. This phenomenon extends the limits of water droplet collision and icing.

(4) The presence of evaporative mass loss significantly reduces the thickness of the leading-edge ice accumulation.

(5) Sobol's sensitivity analysis method can be applied to investigate the extent to which these parameters affect numerical simulations of ice accumulation. The results indicate that: The ice shape parameters of the airfoil's leading edge are most sensitive to icing surface roughness, followed by evaporation and droplet size distribution, with sensitivity to single or multi-shots length being the lowest.

## References

- [1] LANDSBERG B. AOPA air safety foundation: Output and outreach[J]. Aopa Pilot, 2007, 50(5): 79-80.
- [2] JONES S M, REVELEY M S. Subsonic aircraft safety icing study, NASA/TM—2008-215107[R]. Reston, USA: NASA, 2008: 1-45.
- [3] BRAGG M B, LOTH E. Effects of large-droplet ice accretion on airfoil and wing aerodynamics and control, DOT/FAA/AR-00/14[R]. Reston, USA: Illinois Univ At Urbana Dept Of Aeronautical And Astronautical Engineering, 2000: 20-195.
- [4] YUAN Ye. Analysis on the new trend and influence of airworthiness regulations for supercooled large droplets[J]. Science and Technology Innovation and Application, 2015(26): 72.

- [5] COUNCIL A S. GE791 occurrence investigation report, in-flight icing encounter and crash into the sea transasia airways flight 791, ATR72-200, B-22708, 17 Kilometers Southwest of Makung City, Penghu Islands, Taiwan, December 21, 2002 ASC-AOR-05-04-001[R]. Taipei, Taiwan, China: [s.n.], 2002.
- [6] MILLER D, POTAPCZUK M, LANGHALS T. Preliminary investigation of ice shape sensitivity to parameter variations[C]//Proceedings of the 43rd AIAA Aerospace Sciences Meeting and Exhibit. [S. l.]: AIAA, 2005: 73.
- [7] CAMPBELL S E, BROEREN A P, BRAGG M B. Sensitivity of aircraft performance to icing parameter variations[J]. *Journal of Aircraft*, 2007, 44(5): 1758-1760.
- [8] WRIGHT W B. Validation process for LEWICE by use of a Navier-Stokes solver[C]//Proceedings of the 8th AIAA Atmospheric and Space Environments Conference. Washington DC, USA: AIAA, 2016: 4349.
- [9] WRIGHT W B. A revised validation process for ice accretion codes[C]//Proceedings of the 9th AIAA Atmospheric and Space Environments Conference. Denver, USA: AIAA, 2017: 3415.
- [10] SON C, OH S, YEE K. Quantitative analysis of a two-dimensional ice accretion on airfoils[J]. *Journal of Mechanical Science and Technology*, 2012, 26(4): 1059-1071.
- [11] SON C, OH S, YEE K. Quantitative investigation into the relationship between ice accretion shape and ambient conditions[J]. *Transactions of the Japan Society for Aeronautical and Space Sciences*, 2013, 56(4): 175-186.
- [12] HOMOLA M C, VIRK M S, WALLENIUS T, et al. Effect of atmospheric temperature and droplet size variation on ice accretion of wind turbine blades[J]. *Journal of Wind Engineering and Industrial Aerodynamics*, 2010, 98(12): 724-729.
- [13] SHIN J, BERKOWITZ B, CHEN H H, et al. Prediction of ice shapes and their effect on airfoil drag[J]. *Journal of Aircraft*, 1994, 31(2): 263-270.
- [14] ZHU Chengxiang, SUN Zhiguo, FU Bin, et al. The influence of multi-size distribution of water droplets on water droplet impingement characteristics and icing growth[J]. *Journal of Nanjing University of Aeronautics and Astronautics*, 2010, 42(5): 620-624. (in Chinese)
- [15] CAO Yu, WANG Zhengzhi, ZHU Chunling. Numerical simulation of supercooled heavy water droplets icing in engine nacelle[J]. *Aerospace Computing Technology*, 2019, 49(1): 59-63.
- [16] ZHOU Zhihong, YI Xian, DU Yanxia, et al. Research status and development of numerical simulation method of SLD icing[C]//Proceedings of Summary of Papers of the Ninth National Conference on Fluid Mechanics.[S.l.]:[s.n.], 2016.
- [17] LI Haoran, DUAN Yuyu, ZHANG Yufei, et al. Key numerical methods in icing simulation software AERO-ICE[J]. *Journal of Aviation*, 2021, 42(S1): 107-122.
- [18] SARRAZIN F, PIANOSI F, WAGENER T. Global sensitivity analysis of environmental models: Convergence and validation[J]. *Environmental Modelling & Software*, 2016, 79: 135-152.
- [19] SALTELLI A. Global sensitivity analysis: An introduction[C]//Proceedings of the 4th International Conference on Sensitivity Analysis of Model Output (SAMO'04).[S.l.]:[s.n.], 2004.
- [20] IOOSS B, LEMAÎTRE P. A review on global sensitivity analysis methods—Uncertainty management in simulation-optimization of complex systems: Algorithms and applications[M]. Germany: Springer, 2015: 101-122.
- [21] KING D M, PERERA B J C. Morris method of sensitivity analysis applied to assess the importance of input variables on urban water supply yield: A case study[J]. *Journal of Hydrology*, 2013, 477: 17-32.
- [22] LANGSTAFF J, GLEN G, HOLDER C, et al. A sensitivity analysis of a human exposure model using the Sobol method[J]. *Stochastic Environmental Research and Risk Assessment*, 2022, 36(11): 3945-3960.
- [23] HAN J, WU J J, WANG H G, et al. Weight loss function for the cooperative inversion of atmospheric duct parameters[J]. *Atmosphere*, 2022, 13(2): 338.
- [24] WEI W E I, JINGWEN Z, SIJIANG C, et al. Global sensitivity analysis of bullet's angular velocity based on Sobol and EFAST method[J]. *Acta Armamentarii*, 2022, 43(9): 2408-2416. (in Chinese)
- [25] KADKHODAZADEH M, VALIKHAN-ANARAKI M, MORSHED-BOZORGDEL A, et al. A new methodology for reference evapotranspiration prediction and uncertainty analysis under climate change conditions based on machine learning, multi criteria decision making and Monte Carlo methods[J]. *Sustainability*, 2022, 14(5): 2601.
- [26] LYU W, LI Z, ZHANG L, et al. Broadband signal digitization based on low-speed non-uniform photonic sampling[J]. *Photonics*, 2022, 9(11): 831.
- [27] SÁNCHEZ RESTREPO F, HERNÁNDEZ VALDIVIESO A M. Global sensitivity analysis in physiologically-based pharmacokinetic/pharmacody-

- dynamic models of inhaled and opioids anesthetics and its application to generate virtual populations[J]. *Journal of Pharmacokinetics and Pharmacodynamics*, 2022, 49(4): 411-428.
- [28] MANCHALWAR A D, PATNE N R, VARDHAN B V S, et al. Peer-to-peer energy trading in a distribution network considering the impact of short-term load forecasting[J]. *Electrical Engineering*, 2023, 105: 1-13.
- [29] BORMAN R I, AHMAD I, RAHMANTO Y. Klasifikasi citra tanaman perdu liar berkhasiat obat menggunakan jaringan syaraf tiruan radial basis function[J]. *Bulletin of Informatics and Data Science*, 2022, 1(1): 6-13.
- [30] ALATOOM Y I, AI-SULEIMAN T I. Development of pavement roughness models using artificial neural network (ANN)[J]. *International Journal of Pavement Engineering*, 2022, 23(13): 4622-4637.
- [31] GOYAL S. Effective software defect prediction using support vector machines (SVMs)[J]. *International Journal of System Assurance Engineering and Management*, 2022, 13(2): 681-696.
- [32] KOUSHKI M, JABBARI E, AHMADINIA M. Evaluating RBF methods for solving PDEs using Padua points distribution[J]. *Alexandria Engineering Journal*, 2020, 59(5): 2999-3018.
- [33] WANG P, CHEN Z, FENG Y. Many-objective optimization for a deep-sea aquaculture vessel based on an improved RBF neural network surrogate model[J]. *Journal of Marine Science and Technology*, 2021, 26: 582-605.
- [34] SHUAI K, LI Z, ZHOU L, et al. Multi-objective optimization design of PMASynRM based on RBF neural network[J]. *Journal of Physics*, 2022, 2183(1): 012013.
- [35] SHANG X, CHAO T, MA P, et al. Derivative-based global sensitivity measure using radial basis function[J]. *Structural and Multidisciplinary Optimization*, 2020, 62: 107-129.
- [36] BURHENNE S, TSVETKOVA O, JACOB D, et al. Uncertainty quantification for combined building performance and cost-benefit analyses[J]. *Building and Environment*, 2013, 62: 143-154.
- [37] HARDY R L. Multiquadric equations of topography and other irregular surfaces[J]. *Journal of Geophysical Research*, 1971, 76(8): 1905-1915.
- [38] WEN Zheng. MATLAB intelligent algorithm[M]. Beijing: Tsinghua University Press, 2017. (in Chinese)
- [39] RUFF G A, BERKOWITZ B M. User's manual for the NASA Lewis ice accretion prediction code (LEWICE): No. NAS 1.26: 185129. 1990[R]. [S.l.]: NASA, 1990.
- [40] SHIN J, BOND T H. Experimental and computational ice shapes and resulting drag increase for a NACA 0012 airfoil[C]//Proceedings of the Fifth Symposium on Numerical and Physical Aspects of Aerodynamic Flows. Long Beach, USA: NASA, 1992.
- [41] LIU Feiyu, DENG Tian. Influence of dynamic behavior of supercooled large droplets on airfoil icing[EB/OL].[2023-02-21]. <https://doi.org/10.13700/j.bh.1001-5965.2022.0213>.
- [42] CHILTON T H, COLBURN A P. Mass transfer (absorption) coefficients prediction from data on heat transfer and fluid friction[J]. *Industrial & Engineering Chemistry*, 1934, 26(11): 1183-1187.
- [43] RUFF G, ANDERSON D. Quantification of ice accretions for icing scaling evaluations[C]//Proceedings of the 36th AIAA Aerospace Sciences Meeting and Exhibit. [S.l.]: AIAA, 1998: 195.
- [44] SAE. AIR 5666, icing wind tunnel inter facility comparison tests[S]. Washington: SAE Aerospace Information Report, 2012.

**Acknowledgements** This work was supported in part by the Open Fund of Key Laboratory of Icing and Anti/De-icing (No.IADL20200305); and the Scientific Research Project of Tianjin Municipal Education Commission (No. 2020KJ036).

**Author** Dr. DENG Tian received the B.S. and M.S. degrees from Beihang University and Ph.D. degree from Ecole Centrale de Lyon, France. She has been engaged in two-phase flow research for a long time. She is an associate professor with School of Aeronautic Science and Engineering, Civil Aviation University of China. Her research is focused on low pollution emission technology of aero engine, bio-fuel, hydrogen fuel gas engine, complex gas-liquid two-phase flow in aero engine, icing and anti-icing mechanism and application technology direction.

**Author contributions** Dr. DENG Tian designed the study and developed an implementation path. Mr. LIU Feiyu completed the calculations and conducted analysis. Mr. WANG Jiaqi completed the paper. All authors commented on the draft manuscript and approved submissions.

**Competing interests** The authors declare no competing interests.

## 过冷大水滴结冰多参数敏感性分析

邓 甜<sup>1,2</sup>, 王嘉琦<sup>1</sup>, 刘飞宇<sup>1</sup>

(1. 中国民航大学中欧航空工程师学院, 天津 300300, 中国;

2. 中国空气动力研究与发展中心结冰与防除冰重点实验室, 绵阳 621000, 中国)

**摘要:**过冷大水滴结冰现象对飞机的安全运行造成了严重的威胁。本文采用Sobol序列采样法、径向基函数法、Sobol's敏感性指数分析法对结冰表面粗糙度、冰密度、有无蒸发、水滴尺寸分布、步长数进行分析,通过单一参数的一阶敏感性指数表征其对冰形参数的影响程度,通过总敏感性指数比较上述参数之间的相互作用对结冰冰形或结冰量的影响。研究发现,翼型前缘冰形特征参数对上述各参数的敏感性存在一致性规律,均受结冰表面粗糙度影响最大,总敏感指数大于0.476 1,而受步长数影响最小,约为0.2,其余参数的影响程度从大到小依次为蒸发、水滴尺寸分布和冰密度

**关键词:**机翼结冰;过冷大水滴;敏感性分析;冰形特征性参数